THERMAL DESIGN PARAMETERS CRITICAL TO THE DEVELOPMENT OF SOLID FREEFORM FABRICATION OF STRUCTURAL MATERIALS WITH CONTROLLED NANO-LITER DROPLETS

Melissa E. Orme[†] and Changzheng Huang[‡]
[†]Assistant Professor, [‡]Graduate Student
Department of Mechanical and Aerospace Engineering
University of California, Irvine
California, 92717-3975

1. INTRODUCTION

A droplet-based solid freeform fabrication technique for the fast manufacture of *metallic structural* components directly from CAD information is under development. The new technique is similar to StereoLithography in that the final structure is made micro-layer by micro-layer from CAD information. In droplet-based solid freeform manufacturing, metallic structural are fabricated by depositing precisely controlled molten nano-liter droplets [Orme *et al.* 1992] onto a temperature controlled substrate. This paper is aimed at describing the thermal design parameters that are critical to the successful implementation of droplet based solid freeform fabrication.

The unique feature of the technique under development is the fact that the molten droplet streams can be precisely controlled and manipulated. Precise control refers to droplet streams which have an angular stability of the order of *1 micro-radian* [Orme, 1993a], and speed dispersions as low as 3×10^{-7} times the average stream speed [Orme *et al.* 1990]. Droplet generation can be manipulated to produce ultra-uniform droplets at frequencies which would otherwise yield highly non-uniform droplet streams with conventional droplet formation methods (i.e., Rayleigh breakup). Moreover, precise control refers to the ability to "customize" the droplet stream configuration according to the desired material property (i.e., gradient materials) and three-dimensional geometry of the structural component. Customized droplet streams may include streams with two or more droplet sizes and/or separations. The sizes and separations can be predicted (in order of exact occurrence) from a numerical model based on conservation of momentum which requires knowledge of the applied disturbance given to the molten fluid prior to droplet formation [Orme *et al.* 1993b].

Research results presented in this paper deal with droplets formed from a 100 μm orifice, though orifice diameters much smaller could be used in the final realization of the droplet based solid freeform fabrication scheme. A conceptual schematic of the controlled droplet deposition manufacturing technique is shown in figure 1. Molten droplets are ejected from a droplet generator into a controlled environment which may be either a vacuum or a non-reactive gas. As the droplets are formed, they acquire a charge by passing through a charge electrode (not shown). As the charged droplets travel through the deflection electrodes their trajectories are precisely controlled. The charged droplets can be deflected into a gutter for rapid turn-on/turn-off procedures, or they may be deflected onto a substrate for the deposition of fine detailed structures. Details about the droplet generation and charging techniques are given elsewhere [Orme *et al.* 1995a]. As the droplets travel they convect heat. The degree of convection is governed by the initial temperature of the droplets, droplet speed and the environment background pressure and temperature (see section 3.3). Upon arrival at the substrate, they undergo a "splatting" action which entails simultaneous spreading and solidification. Under certain circumstances when the droplets have partially pre-solidified due to convection prior to impact, the solidified droplet profile will be nearly spherical. In other realizations the solidification time may be long compared to the spreading time, and the solidified droplet profile will approximate the shape of a short cylinder. Successive droplet deliveries build the 3-D structural component. Methods of controlling the thermal conditions in order to insure that the

thermal energy content of incoming droplets is sufficient to remelt a thin layer of the previously solidified deposit are described in sections 3.3 and 3.4. The remelting scheme is advantageous because it will enable a layer on the surface of the previously deposited and solidified material to unite in the molten phase with incoming material so that individual splat boundaries will become obliterated, leading to a homogeneous structural component.

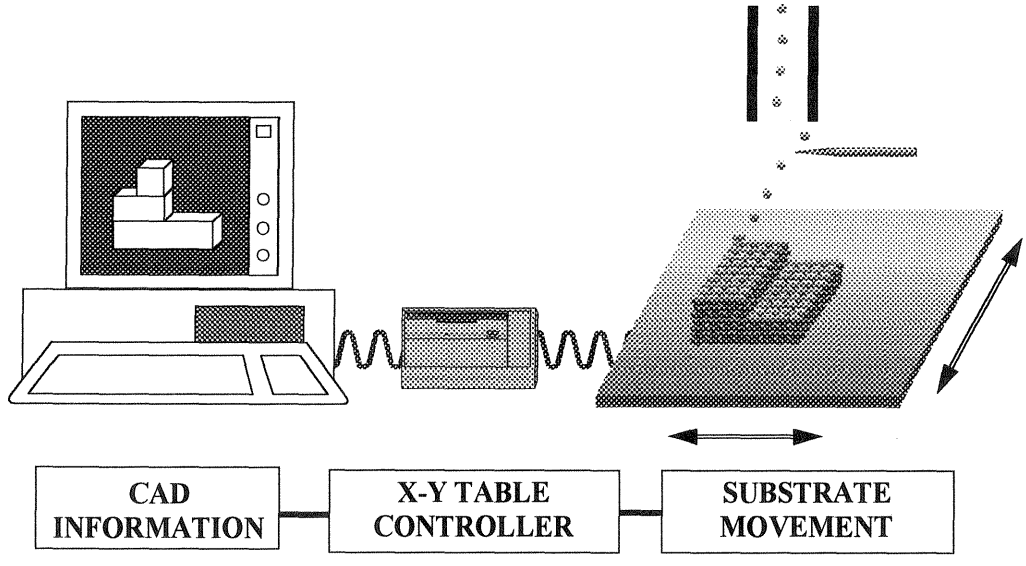

Figure 1: Conceptual Schematic of droplet-based solid freeform fabrication technique.

1.1 DROPLET FORMATION

Droplet formation from capillary streams is typically achieved by application of the well-known Rayleigh instability [Lord Rayleigh, 1878]. Rayleigh developed the first quantitative theory which describes the wave motion on a liquid jet. For sake of this discussion, we assume that molten metal is issued through an orifice of radius r_o. A controlled periodic disturbance is initiated on the surface of the jet by means of a mechanical vibration. Lord Rayleigh developed the first linear stability analysis where he considered an infinitely long, circular, inviscid jet subject to a temporal disturbance growth. He found that disturbances of the radius grow in time t as $e^{\beta t}$, where β is the growth rate of the disturbance given for a viscous fluid by Weber [1931] as:

$$\beta^2 + \frac{3\nu k_o^{*2}}{r_o^2}\beta = \frac{\sigma}{2\rho r_o^3}\left(1 - k_o^{*2}\right)k_o^{*2} + \frac{V_o \hat{\rho} k_o^{*2} K_o(k_o^*)}{2r_o^2 \rho K_1(k_o^*)} \tag{1}$$

Where K_n is the nth order modified Bessel function of the second kind, $\hat{\rho}$ is the density of the ambient fluid, ν is the kinematic viscosity of the fluid, σ is its surface tension, and k_o* is the nondimensional wavenumber equal to $2\pi r_o/\lambda$, where λ is the wavelength of the disturbance. The above relation predicts that the surface disturbance on a capillary stream is unstable and results in droplet formation for $k_o^* < 1$.

1.1.1 Droplet Formation at Extended Wavelengths and Pattern Formation

Molten metal droplets used for solid freeform fabrication of metallic parts can be generated with amplitude modulated disturbances in order to increase the uniformity of the droplet speeds (beyond 1×10^{-6}) and to extend the wavelength beyond that dictated by conventional Rayleigh breakup [Orme, 1990]. When using amplitude modulated disturbances for droplet generation, the fast, or "carrier" frequency is given by Rayleigh-mode break-up as described above, and the modulation frequency is either (1) an integral multiple

of the carrier frequency for the generation of ultra-uniform droplets at extended wavelengths, or (2) a non-integral multiple for the generation of poly-dispersed droplets.

Figure 2 illustrates molten droplet configurations generated with amplitude modulated disturbances. Figure 2a presents a droplet stream generated with the conventional mode described above. Figure 2b and 2c illustrate droplet configurations generated with amplitude modulated disturbances with frequency ratios of N=2 and 3. In previous work, it was found that the speed dispersion of amplitude modulated disturbances decreases as $1/N$, where N is the frequency ratio of the amplitude modulated disturbance [Orme *et al.* (1990)].

The generation of controlled poly-dispersed droplet streams could also find application in materials synthesis with ultra-uniform droplet deposition. An example includes use of smaller droplets to fill in the interstices left by the deposition of the larger droplets. Controlled poly-dispersed droplet streams are those in which the droplet sizes and separations can be varied and controlled (see Orme [1993b] for more details). An example of a droplet pattern is shown in figure 2d. In this realization the droplet parameters of orifice diameter, background pressure, stream speed, and carrier frequency are identical to those in figures 2a-c. The modulation frequency is 1/3.5 times that of the carrier frequency. Note that the smaller droplets in-between the larger droplets are not satellite droplets and will not merge with either droplet over long distances (order of 10 m). Spectral analysis over 128,000 droplets illustrates a time-invariant droplet stream.

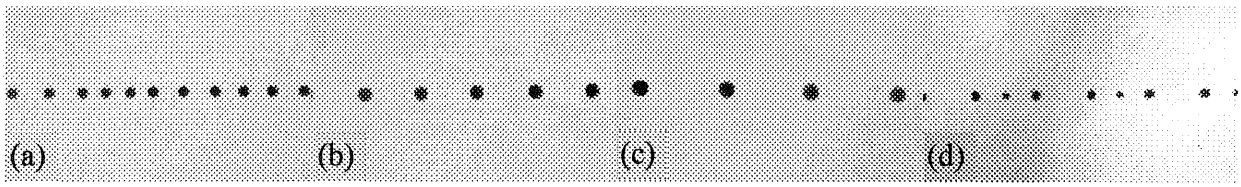

Figure 2: Droplet stream configurations generated from a 100 μm diameter orifice and a stream speed of 4.8 m/s. (a) conventional droplet generation, (b) -(c) generated with amplitude modulated disturbances with frequency ratios N=2, 3 and 3.5 respectively.

2. INITIAL DEMONSTRATIONS

The droplet streams illustrated in figure 2 were composed of molten lead/tin alloy. Extensive research results on droplet control and manipulation described in the previous section provides the basis for the solid freeform fabrication concept. Several droplet freeforms have been fabricated from the low melting point lead/tin alloy. The critical information gained from these studies is that (1) structures with thickness' at least up to 1000 splats high can be deposited; (2) under selected conditions, the deposits can exhibit porosities as low as 0.03%; and (3) the deposits have a significantly refined microstructure over the cast counter-part, thereby yielding a higher structural quality of the component.

Preliminary experiments have also been conducted with molten aluminum droplets (though not as extensively as with the low melting point alloys), and initial results indicate that the droplet formation phenomenon (excepting the reactive nature of the molten aluminum) is identical to that for the lower melting point metals. Figure 3a shows a micrograph of the aluminum droplet based solid freeform fabricated sample, and 3b illustrates the aluminum cast counterpart. The cross section pictured in 3a shows the top fraction of a millimeter of the deposit which is composed of approximately 15-20 splats edge on. It can be seen that the droplet deposited aluminum has a significantly refined microstructure over its cast counterpart, and that splat boundaries have been obliterated by droplet remelting. In these results, the remelting action was for the most part uncontrolled and the remelt depth varied with height of the freeform. This paper addresses the issue of controlling the remelting action in an effort to control the microstructure

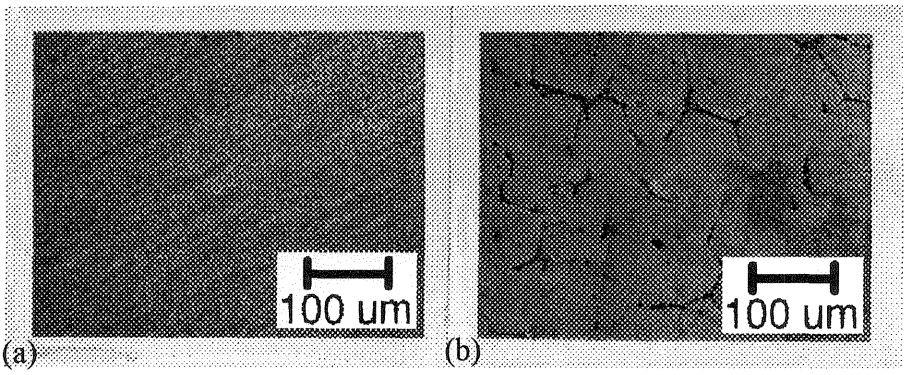

Figure 3: (a) Microstructure of preliminary aluminum droplet deposited part. (b) Microstructure of aluminum cast part shown as a comparison. Magnification is the same in both micrographs.

further. Even though the development of the process is in its infancy, significant gains have been made on the microstructural integrity of the components.

3. CRITICAL CONTROL PARAMETER CONSIDERATIONS

As described in the Background section, there exists only a certain range of droplet production frequencies which will yield uniform droplet generation. For inviscid fluids (such as liquid metals) the frequency which yields most uniform droplet behavior is found at k_0*=0.697, which is the k_0* of maximum in the growth rate given by equation (1) [Orme (1991)]. Recalling that the nondimensional wavenumber, k_0*, is given by $2\pi r_0/\lambda$, where r_0 is the initial stream radius and λ is the wavelength of the disturbance, the frequency of most uniform droplet production can be determined. For molten aluminum droplet streams emanating from a 25 and 100 micron diameter orifices at 8m/s, the droplet production frequencies are 70,995 and 17,857 droplets/second respectively. The droplet radius r_d is found from conservation of mass. Orifice diameters of 25, 50 and 100 microns will yield droplet diameters of 47, 94, and 189 microns respectively when generated with k_0*=0.697. For conditions discussed above, a droplet stream composed of droplets 47 μm stream traveling at 8m/s, the material throughput is .0038 cc/s, and the mass flow rate is 0.54 grams/minute. For 189 micron diameter droplets traveling with the same conditions, the material throughput and mass flow rate are .062 cc/s and 8.8 grams/minute!

3.1 EFFECTS OF AERODYNAMIC DRAG

Molten droplets are injected into either a vacuum or a controlled environment of nonreactive gas. For charging and deflection considerations, it is attractive to inject the droplet stream into a stagnant inert gas. When the droplets travel in the inert gas, they experience a deceleration due to aerodynamic drag. The deceleration will significantly alter their electrostatic deflection and convective heat transfer characteristics. We can estimate the effect of aerodynamic drag on the droplet by considering the following equation of motion:

$$mg - C_D \cdot \frac{1}{2}\rho_s v^2 = m\frac{dv}{dt} \tag{2}$$

Where ρ_s is the density of the surroundings, v is the droplet speed, C_D is the drag coefficient, g is the gravitational constant, and m is the droplet mass. For a spherical droplet, the drag coefficient is related to droplet speed by [White (1991)]:

$$C_D = \frac{24}{Re} + \frac{6}{1+\sqrt{Re}} + 0.4 \tag{3}$$

Where Re is the Reynolds number equal to $\rho vd/\mu$, where d is the droplet diameter and μ is the dynamic viscosity of the nitrogen environment. Equations (2) and (3) are combined and numerically integrated to solve for the time varying droplet speed.

3.2 DROPLET CHARGING AND DEFLECTION

Droplet charging and deflection offers a flexible approach to droplet deposition for solid freeform fabrication. Charged droplets can be selectively positioned onto a substrate, or into a gutter for rapid turn-on/turn-off maneuvers. An example of a charged droplet stream is shown in figure 4. Here the molten droplets are 189 microns in diameter, the charge electrode was given a sinusoidal voltage with a peak to peak voltage of 400V applied over .5cm, and the deflection plate potential was 6×10^5 V/m. The droplets were charged by passing the jet through a charge electrode at the point of droplet formation. The electrode is centered about the jet axis at the stream breakup point. The molten jet is grounded, and a positive potential is applied to the charge electrode. The amount of charge given to the droplet is determined by the level of voltage applied to the electrode at the time of droplet formation.

A predictive model for the deflection is included elsewhere [Orme (1995a)]. The results from that model show that for the conditions stated above, 189 micron droplets are deflected approximately 2 cm after a vertical flight distance of 20cm. Decreasing the droplet diameter increases the charge to mass ratio on the droplet, thereby giving higher deflections. For droplets formed from a 50 micron orifice, a deflection of 12 cm is predicted after a vertical distance of 20 cm. For smaller droplets (47 micron in diam.) formed from a 25 micron orifice, extreme aerodynamic drag competes with the higher charge to mass ratio, creating the nonlinear behavior in deflection as a function of travel distance.

Figure 4: Example of droplets which are charged and deflected by issuing them into a sinusoidally varying deflection field. Droplet diameters are 189 μm.

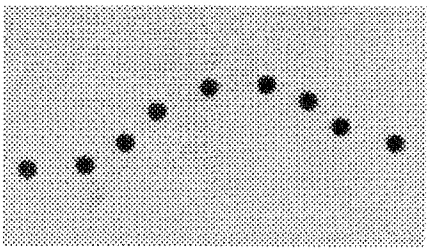

3.3 DROPLET CONVECTION IN FLIGHT

For the conditions described in this work, Biot <<1, so variation of temperature within the droplet during transients is less than 5% [Özisik, 1993], and the following lumped system formulation is valid:

$$h(t)A(T_\infty - T) = \rho_\ell C_{p\ell} V \frac{dT}{dt} \tag{4}$$

Where $h(t)$ is the heat transfer coefficient which varies in time due to aerodynamic deceleration, A is the surface area and V is the volume of the droplet, ρ_ℓ is the density of the liquid phase, $C_{p\ell}$ is the specific heat capacity of the liquid phase, and T_∞ is the ambient temperature.

The heat transfer coefficient is coupled to the velocity through the Reynolds number, Re, in the Ranz Marshall relation [Poirier and Geiger 1994]:

$$Kn = \left(2 + .6\sqrt{Re}\, Pr^{1/3}\right) \tag{5}$$

Where Kn is the Knudsen number equal to hd/k, k is the thermal conductivity of the surrounding fluid, and Pr is the Prandtle number of the surrounding fluid equal to α/ν, where α is the thermal diffusivity of the droplet material equal to $k/(\rho C_p)$, and ν is the kinametic viscosity. The temperature drop described by equation (4) is numerically integrated to include the effects of droplet deceleration.

3.4 MOVING BOUNDARY HEAT CONDUCTION

In this section we describe the numerical simulations of heat conduction with a moving boundary through the molten material. With knowledge of the droplet arrival temperature at the substrate, it is possible to track the solid/liquid interface as it moves towards the upper surface of the splat. We assume that the solidification takes place in the liquid because of the presence of the cold substrate. We also assume that the splat has spread to a short cylinder prior to the onset of solidification. The latter assumption can be unrealistic for many actualizations depending on droplet speed and temperature difference between the droplet and the substrate. For circumstances of interest in this work, it is desired to deliver the droplets with high enough thermal energy to remelt a micro-layer of the previously deposited material. Therefore, with the aforementioned thermal conditions, it is not unreasonable to assume that the droplet will assume the shape which approximates a short cylinder prior to the onset of solidification. For other applications which require droplet delivery at the substrate with a temperature which would not allow complete spreading, a more realistic model must be developed which includes the formidable task of coupling the Navier-Stokes equations of momentum with the transient heat conduction model in order to simulate the phase change through a deforming droplet.

To simulate the moving boundary heat conduction problem, we use the 1-D Stephan problem for the solidification portion of the problem as outlined in Carslaw and Jaeger [1959]. The interface condition is determined by considering an interface energy balance at $x=s(t)$ and assuming that the difference in conduction through the liquid and solid phases is equal to the rate of heat liberated during solidification. At time t=0, a droplet makes contact with a substrate whose lower boundary is maintained at temperature T_{sub} at all times. The arriving molten liquid causes a thin layer of the previously deposited material to remelt, erasing the boundary between the remelt zone and the newly deposited droplet. The liquid/solid interface defined by $s(t)$ travels through the molten material until it reaches the upper surface of the splat. We assume that the phase transition takes place at the unique temperature T_m, i.e., that no undercooling occurs, and the two phases are separated by the sharp interface. Convection effects in the liquid phase are ignored. For the sake of brevity, the details of the analysis are described qualitatively. A more complete description of the numerical analysis approach is given elsewhere [Orme (1995b)].

3.4.1 Solidification

We seek a strategy for which the thermal energy content of the incoming molten droplets is sufficient to remelt the previously solidified material. To simulate the solidification aspects of the problem, we use a central difference scheme which is implicit in time in order to discretize the 1-D moving boundary problem.

3.4.2 Remelting

When remelting takes place, the numerical method used for solidification may suffer from non-convergence near the melt interface under certain circumstances. Therefore, for the remelting simulations, we have transformed the moving boundary into a fixed boundary problem with the following transformation:

$$\eta = \frac{M - s}{s\left[s - (M+1)\right]} x^2 + \frac{s^2 - M(M+1)}{s\left[s - (M+1)\right]} x \tag{6}$$

Where M is the number of splats previously deposited, s is the solid portion of the material (material thickness minus the remelt zone), and x is the distance through the material with $x=0$ defining the aluminum/copper substrate interface, and $x=(M+1)a$ defining the top surface of the deposited material where a is the splat thickness. Using the transformation, the governing equations for the liquid and solid

state is recast into the fixed reference frame, and a central difference scheme is employed to simulate the remelting process.

3.4.3 Cooling

Following remelting, the molten material solidifies according to the framework outlined previously. The splats cool prior to subsequent droplet deposition. Cooling is simulated with the Crank-Nicolson regime [Croft and Lilley (1977)].

4. RESULTS AND DISCUSSION

Figure 5 illustrates the solid/liquid interface through four splats which are each 10 μm thick. It can be seen that the first splat solidifies in a time approximately equal to 1.4 μs. Droplets are delivered successively every 56 μs, which corresponds to the frequency of most uniform droplet generation as discussed in the Background section of this paper. Delivery of the subsequent droplet causes local remelting, as can be seen by the reversal of direction in the solid/liquid interface. The remelted zone was fixed at 1 μm in the simulations. Remelting action causes the interface between the remelted zone and the incoming molten droplet to become erased. Conduction causes the molten metal to solidify, as depicted by the following change in direction of the solid/liquid interface as it travels upward toward the top surface of the splat. The process is repeated until the final freeform is deposited.

Figure 6 illustrates the variation in incoming temperature required as a function of number of splats delivered in order to achieve a constant remelt depth of 1 μm. The time between successive droplet deliveries was varied in the simulation from 28 μs to ∞. Increasing the time between droplet deliveries is equivalent to increasing the area to be deposited. Assuming that the droplets are still generated at 56 μs, they can be rastered back and forth, so that they impinge on the same location at a lower frequency.

Figure 7 illustrates the effect of substrate temperature on the remelting phenomenon. Each curve describes the temperature above the melting point required for the incoming droplets to remelt a zone 1 μm thick for a droplet delivery rate of 56 μs. The curves indicated by the "+", "*", and "x"symbols correspond to substrate temperatures of 20, 120, and 220 ^{0}C respectively. Hence, in order to make the strategy more practical, it is attractive to heat the substrate moderately.

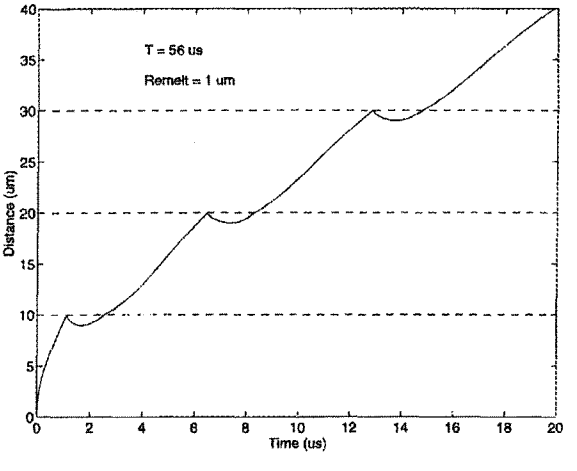

Figure 5: Solid/liquid interface through four splats which are each 10μm thick. Deposition frequency is 56μs, and remelt zone is fixed to 10μm.

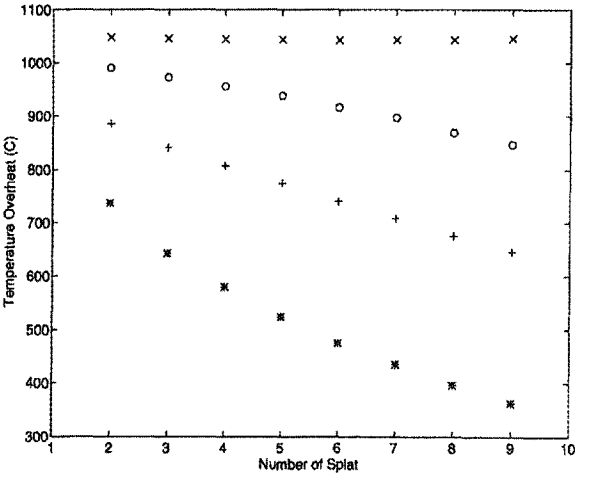

Figure 6: Temperature required to remelt a zone of 1μm. Deposition frequency is varied from 28 μs(*), 56 μs (+), 112 μs (o), to infinite time (x).

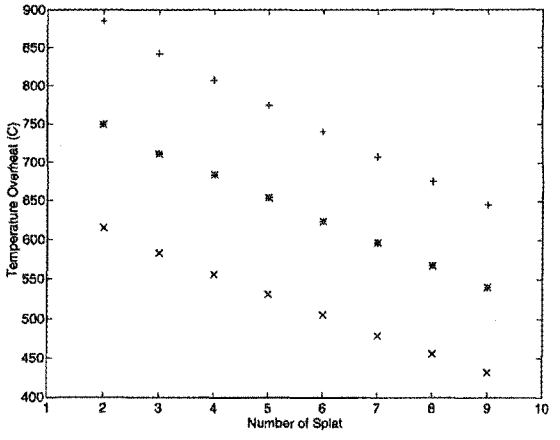

Figure 7: Temperature above melting point required to remelt a zone of 1 μm. Deposition frequency is 56 μs. Lower surface of substrate is 20, 120, and 220 ^{0}C respectively for +, *, and ×.

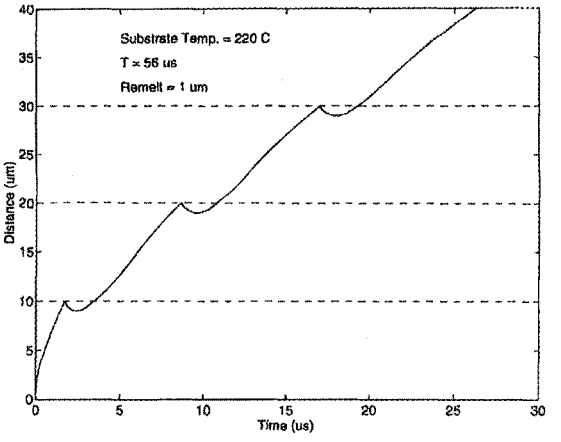

Figure 8: Solid/liquid interface through four splats which are each 10 μm thick. Droplet deposition frequency is 56 μs, and lower surface of substrate is held constant at 220 ^{0}C.

Figure 8 illustrates the solid/liquid interface through four splats which are each 10 μm thick. In this case, the time between successive droplet depositions to the fixed location is 56 μs, and the lower surface of the substrate is fixed at 220 ^{0}C. It can be seen the droplets are still rapid solidifying, even though the substrate temperature is increased.

In summary, a thermal strategy for remelting the solidified material in droplet-based solid freeform fabrication has been outlined. The strategy allows the flexible deposition of molten metal droplets to be decoupled from the solidification history of the previous layer of droplets. Remelting will insure that the microstructure of the freeformed part is refined, and with low porosity. In cases when it is practical to vary the droplet temperature, the remelt zone can be fixed to a constant depth. In an effort to reduce the superheat necessary, the substrate temperature can be increased above room temperature, without significantly jeopardizing the rapid solidification time.

ACKNOWLEDGMENTS

The authors acknowledge NSF grants DMI-9396221 and DMI-9457205 for support, as well as the generous equipment contributions from the Delphi Interior and Lighting Division of General Motors. The authors also thank Mr. Ken Willis and Mr Jon Courter for their help in taking photographs.

5. REFERENCES

Carslaw, H.S. & Jaeger, J.C. [1959] *Conduction of Heat in Solids,* Oxford Science Publications

Croft, D.R. & Lilley, D.G. [1977] *Heat Transfer Calculations,* Applied Science Pub., London

Orme, M.E. and Muntz, E.P. [1992] U.S. Patent Number 5,171,360.

Orme, M.E. [1993a] *SAE Technical Paper Series 932566,* Aerotech '93, September 27-30

Orme, M [1991] *The Physics of Fluids A,* **3,** (12)

Orme, M.E., and Muntz, E.P. [1990] *The Physics of Fluids A,* **2,** (7)

Orme, M.E., Willis, K., and Nguyen, T-V [1993b] *The Physics of Fluids A,* **5,** (1)

Orme, M.E., and Huang, C. [1995a] submitted to *J. Atomization and Sprays*

Orme, M.E., and Huang, C. [1995b] submitted to *J. Heat Transfer*

Özisik, M.N. [1993] *Heat Conduction* Wiley Inter-Science

Poirier D.R. and Geigre G.H. [1944] *Transport Phenomena in Materials Processing,* TMS publishing

Rayleigh, Lord, [1879] On the instability of jets. *Proc. London Math. Soc.* **10,** 4-13

Weber, C. [1931] Zum zerfall eines flussigkeitsshahies, *Z. Angew. Math. Mech.* **11,** 136

White, F.F. [1991], *Viscous Fluid Flow,* McGraw Hill, 2nd edition.